PERGAMON

International Journal of Heat and Mass Transfer 41 (1998) 3409–3430

International Journal of HEAT and MASS TRANSFER

Momentum and heat transfer from cylinders in laminar crossflow at $10^{-4} \leqslant Re \leqslant 200$

C. F. Lange, F. Durst*, M. Breuer

Institute of Fluid Mechanics, University of Erlangen-Nürnberg, Cauerstr. 4, D-91058 Erlangen, Germany

Received 23 July 1997; in final form 3 February 1998

Abstract

A summary of results of numerical investigations of the two-dimensional flow around a heated circular cylinder located in a laminar crossflow is presented. Numerical investigations were carried out for the Reynolds number range $10^{-4} \leqslant Re \leqslant 200$ and for temperature loadings of 1.003–1.5. The computations yield information on Nu and C_D variation with Reynolds number. The temperature dependence of the fluid properties (air) was taken into account and this resulted in a temperature dependence of the Nu–Re and C_D–Re results. Information is also provided on the Strouhal number dependence on the Re number and on the critical Re number where vortex shedding starts.

Nomenclature

C_D drag coefficient
C_L lift coefficient
c_P specific heat at constant pressure
D cylinder diameter
Ec Eckert number
f vortex shedding frequency
$\boldsymbol{g}$ gravitational acceleration
Gr Grashof number
H outer dimension of computational domain
h_c heat transfer coefficient
k thermal conductivity
Kn Knudsen number
L molecular mean free path
Ma Mach number
Nu Nusselt number
P pressure
Pr Prandtl number
$\dot{q}$ specific heat flux
Re Reynolds number
St Strouhal number
T temperature
U_i cartesian velocity components
x_i cartesian coordinates.

Greek symbols

β coefficient of volumetric thermal expansion
γ specific heat ratio
Γ Euler constant
$\varepsilon_{H/D}$ discretization error due to the domain size
μ dynamic viscosity
ν kinematic viscosity
ρ fluid density
τ temperature loading
Φ viscous dissipation function.

Subscripts

∞ free stream region
f at arithmetic mean (film) temperature
m integrated mean property value
w at the cylinder wall.

Superscript

* nondimensional quantity.

1. Introduction

The laminar, two-dimensional flow around a circular cylinder located in a spatially and time constant velocity field has been of continuous interest to researchers involved in basic fluid mechanics. Almost every standard textbook on fluid dynamics describes the different flow

* Corresponding author.

0017–9310/98 $19.00
PII: S0017–9310(98)00077–5

structures and the resultant change of the drag coefficient as a function of the Reynolds number; see, e.g., Schlichting and Gersten [1]. However, most experimental studies have investigated the C_D–Re correlation at high Reynolds numbers. There are comparatively few reliable experimental investigations available on the drag of the cylinder for moderate, low and very low Reynolds numbers. The classical studies covering this range of Re numbers, see e.g. [2–6], show a relatively large scatter of the results. In these older investigations the discrepancies increase with decreasing Re, owing to experimental limitations introduced by the accuracy of the force measurements at low values of Re. Only recently have better experimental results become available. Unfortunately, the relative recent and more accurate results of Huner and Hussey [7] are limited to low values of the Re number ranging from 0.2–2.6 only, owing to experimental limitations. These limitations demand the employment of analytical and numerical techniques to yield reliable information on the drag coefficient of the circular cylinder flow over the wide range of Re covered in this study.

A somewhat different situation exists for the experimental investigation of the heat transfer from a cylinder at low and moderate Reynolds numbers. Mainly motivated by the need of heat transfer in hot-wire anemometry to correlate the heat loss from the wire probe with the flow velocity, numerous studies have been carried out on this topic. The early work of King [8] provided results in terms of the heat transfer coefficient and was published one year before Nusselt [9] suggested the use of the nondimensional number, that is nowadays known by his name, to present heat transfer data. Subsequent investigators focused on the correlation of the Nusselt number with the Reynolds number, e.g. [10–14]. As in the case of C_D, the Nu–Re plots of the experimental investigations show a large scatter in the data. This is in part caused by the inappropriate treatment of the variation of fluid properties with temperature. In the range of very low Reynolds numbers ($Re < 0.1$), the scatter in the results is also due to natural convection effects.

Recently, the von Kármán vortex street, generated in the wake of the cylinder at moderate Reynolds numbers ($Re \gtrsim 46$), has gained increasing interest. Whereas in the past, mainly two-dimensional flow visualizations were reported in the literature, recent flow visualization experiments provided a better understanding of the three-dimensional effects in the wake caused by the cylinder ends. This gave rise to various experimental investigations of this flow regime. Williamson [15] summarized recent advances on this subject. His summary made it clear that there is also a need for more detailed information on the pure two-dimensional vortex shedding mode of cylinder flows, which is difficult to isolate in experiments, but can be reliably investigated by numerical simulation.

Analytical investigations of the laminar, two-dimensional flow around a circular cylinder at low Re numbers go back to the early work carried out by Stokes [16]. He linearized the equations for the flow at very low Reynolds numbers about the vicinity of the cylinder. He found that the resulting boundary value problem had not solution. This is known as the Stokes paradox. Many years later, Oseen [17] explained that this paradox resulted from the neglect of the nonlinear inertia terms, which become dominant far from the cylinder. He suggested that the problem could be avoided by linearizing the flow equations at infinity and thereby partially taking the inertia terms into account. Soon thereafter, Lamb [18] found a solution of Oseen's equations for a circular cylinder which employed an approximate boundary condition at the surface. It provided a first approximation of the flow around the cylinder and an analytical expression for the drag. Tomotika and Aoi [19] later derived an expansion formula for the drag, based on their extended solution of Oseen's equations.

Much later, Proudman and Pearson [20] and Kaplun [21] showed that the problem could be solved to any order of the terms by matching two asymptotic expansions which are valid near to and far from the cylinder, the 'Stokes' and the 'Oseen' expansions, respectively. Further extensions of the method of matched asymptotic expansions and better results in the region of $Re \approx 1$ were presented by Tamada et al. [22] and Keller and Ward [23].

The heat transfer from circular cylinders has also been the subject of analytical investigations, but these studies have not been as intensive as those involving the drag. The pioneering work of Cole and Roshko [24] on the heat transfer from a cylinder in crossflow was based on Oseen's approximation for the flow field, which was applied to the thermal energy equation for low temperature differences (constant fluid properties). They found the first term of an expansion in $[\ln (Re\,Pr)]^{-1}$ for the Nusselt number. Wood [25] extended the work of Cole and Roshko [24], determining two additional terms in the Oseen expansion of the velocity and temperature fields. Hieber and Gebhart [26] obtained a similar solution matching two asymptotic expansions of the temperature and employing the flow solution of Kaplun [21] and Proudman and Pearson [20].

All the theoretical efforts cited above already faced extreme difficulties in treating flows past a cylinder at low to moderate Reynolds numbers, i.e. for $Re \gtrsim 2$. Hence there are at present insufficient analytical results available to add reliable information to the experimental findings of the laminar, two-dimensional flow around circular cylinders at $Re \gtrsim 2$. The situation described readily suggests that numerical investigations are the only means to investigate successfully the flow past circular cylinders over a wide range of Reynolds numbers, where either the experimental or the analytical methods fail to provide accurate information on the flow field and on integral

flow properties. This is particularly the case when flows around heated cylinders with larger temperature differences are considered and variable fluid properties need to be taken into account. These observations triggered the work summarized in this paper.

The early numerical studies of the flow around circular cylinders used in general a stream function-vorticity formulation of the equations. Thom [27] presented the first published calculation on the flow past a cylinder at Reynolds numbers of 10 and 20. Later, Kawaguti [28] integrated the stream function and the vorticity equations for a Reynolds number of 40. These pioneering papers reported computations carried out manually. The latter took, for example, 18 months to perform 10 iterations. In the next decade, the first unsteady calculations of the impulsively started symmetric flow around a circular cylinder (Kawaguti and Jain [29], Ingham [30]) and the first investigations of the effect of the domain size (Keller and Takami [31]) appeared, together with the use of computers for the calculations. However, the unsteady computations at that time were restricted to time marching of the solution starting from the fluid at rest up to the steady-state solution.

Perhaps the first unsteady computation of the cylinder wake was the work of Fromm and Harlow [32], who demonstrated successfully the development of the von Kármán vortex street using cyclic boundary conditions at the inflow and outflow borders. Later, Thoman and Szewczyk [33] computed transient solutions for a wide range of Re from 1 to 10^5. In addition to the drag, usually the pressure distribution, streamlines and vorticity contours were presented for some Reynolds numbers. The number of papers on numerical computation of the flow past a cylinder grew fast with time. The main reason was the attraction of this physical problem, with rather simple geometry, but complicated flow structure. Many new developed numerical techniques and their variations were tested using the cylinder flow. With few exceptions, like Sucker and Brauer [34], most of the investigations did not really study the physical aspects of the flow, but were merely interested in the validation and demonstration of the abilities of the computer codes employed. With recently increasing interest in the onset of the von Kármán vortex street and its instabilities, many numerical investigations have been carried out on this subject, e.g. [35–40]. On the other hand only a few numerical investigations dealing with very small Reynolds numbers ($Re < 0.1$) are available.

Compared with the isothermal flow past a cylinder, there are remarkably few publications on the numerical solution of the heat transfer from a cylinder in crossflow. The available publications describe the study of pure forced convection, e.g. Dennis et al. [41] and Sucker and Brauer [42], the influence of buoyancy, e.g. Ho et al. [43], Sundén [44] and Hatanaka and Kawahara [45], or the influence of viscous heating on forced convection, e.g. Sundén [46].

The availability of very efficient flow simulation codes (block structured, finite volume method), the advances in numerical methods (multi-grid method, local grid refinement) and the addition of computer power (parallel scalar and vector computers) have provided computational fluid dynamics with the maturity to compete with the classical investigation methods with the same level of accuracy, but with more flexibility in the specification of flow parameters. The joint progress of the three pillars of CFD delivered the necessary capacity to conduct detailed and accurate investigations on the laminar two-dimensional flow past heated circular cylinders covering a wide range of Reynolds numbers. To the best of the authors' knowledge, there has been no previous numerical investigations to a similar extent on this physical problem.

2. Basic equations and their solution

2.1. Basic equations

In the present study investigations are restricted to cases, where continuum mechanics and incompressibility can be assumed. The governing nondimensional equations for an incompressible two-dimensional flow expressing the conservation of mass, momentum and energy are as follows:

$$\frac{\partial}{\partial x_i^*}(\rho U_i^*) = 0 \tag{1}$$

$$St\frac{\partial (U_j^*)}{\partial t^*} + U_i^*\frac{\partial (U_j^*)}{\partial x_i^*} = -\frac{\partial P^*}{\partial x_j^*} + \frac{1}{Re}\frac{\partial}{\partial x_i^*}\left[\mu^*\frac{\partial U_j^*}{\partial x_i^*}\right] + \frac{Gr}{Re^2}T^* \tag{2}$$

$$St\frac{\partial T^*}{\partial t^*} + U_i^*\frac{\partial T^*}{\partial x_i^*} = \frac{1}{Re\,Pr}\frac{\partial}{\partial x_i^*}\left[k^*\frac{\partial T^*}{\partial x_i^*}\right] + \frac{Ec}{Re}\Phi^* \tag{3}$$

where $(i,j = 1,2)$, U_i^* are the cartesian velocity components normalized with the free stream velocity U_∞ and x_i^* are the cartesian coordinates normalized with the cylinder diameter D, t^* is the time normalized with the vortex shedding frequency f, P^* is the pressure normalized with $\rho_\infty U_\infty^2$, μ^* and k^* are the dynamic viscosity and the thermal conductivity, respectively, normalized with the corresponding value at the free stream temperature, T^* is the temperature normalized with the temperature difference between the cylinder surface and the undisturbed flow $(T_w - T_\infty)$ and Φ^* is the normalized viscous dissipation function given by

$$\Phi^* = \left(\frac{\partial U_i^*}{\partial x_j^*} + \frac{\partial U_j^*}{\partial x_i^*}\right)\frac{\partial U_i^*}{\partial x_j^*}. \tag{4}$$

The nondimensional parameters relevant to the considered flow problem are

$$\text{Strouhal number}: St = \frac{fD}{U_\infty}$$

$$\text{Reynolds number}: Re = \frac{\rho_\infty U_\infty D}{\mu_\infty}$$

$$\text{Prandtl number}: Pr = \frac{\mu_\infty c_{P\infty}}{k_\infty}$$

$$\text{Eckert number}: Ec = \frac{U_\infty^2}{c_{P\infty}(T_w - T_\infty)}$$

$$\text{Grashof number}: Gr = \frac{D^3 \boldsymbol{g} \beta \rho_\infty^2 (T_w - T_\infty)}{\mu_\infty^2}$$

where $\boldsymbol{g}$ is the gravitational acceleration, β the coefficient of volumetric thermal expansion, ρ_∞ the density and $c_{P\infty}$ the specific heat at constant pressure, both evaluated at the free stream temperature.

In the case of small temperature differences between the cylinder and the undisturbed flow, the fluid properties may be treated as constant. Consequently, in the computations described in Section 3 the nondimensional properties μ^* and k^* are set to unity. Owing to the dimensions and temperatures involved in the present investigation, natural convection and viscous dissipation effects are negligibly small. Therefore, the last terms in equations (2) and (3) were neglected in the present computations. In the next section, these simplifications of the general equations will be addressed and justified.

2.2. Justification of assumptions

In the present study, the computations concentrate on convection-dominated flows for which the assumptions of incompressibility and continuum apply. In the following, explanations are presented regarding the validity of these assumptions. It will also be shown that the ranges of dimensions, velocities and temperatures adopted in this investigation allow the neglect of viscous dissipation and natural convection effects.

The validity of the continuum assumption is by no means obvious, considering the small dimensions of cylinders involved in the present investigation. At the lower values of Reynolds numbers ($Re \approx 10^{-4}$) very small cylinders (down to $D = 0.5$ μm) are needed in order to reduce the influence of buoyancy, as will be discussed later. The computation with such small cylinders, although numerically feasible, reaches the limits of the physical model, when the no-slip condition and the continuous temperature distribution at the cylinder wall ceases to apply. Both conditions are based on the assumption of continuum, corresponding to small values of the Knudsen number, which is defined as

$$Kn = \frac{L}{D} = \left(\frac{\gamma\pi}{2}\right)^{1/2} \frac{Ma}{Re} \tag{5}$$

where L is the molecular mean free path, γ the specific heat ratio and Ma the Mach number given by $Ma = U_\infty/c$, where c is the speed of sound in the fluid. In the present case the value of Kn is about 0.1 for the smallest cylinder in an air flow.

Collis and Williams [12] analyzed the effect of temperature jump at the cylinder wall. They showed that the relation between the measured value of the Nusselt number, Nu_{meas}, and the value corrected for continuum, Nu_{cont}, in the case of a platinum wire in a crossflow of air is approximately

$$\frac{1}{Nu_{cont}} = \frac{1}{Nu_{meas}} - 2Kn. \tag{6}$$

This means that an experiment with a platinum wire of 0.5 μm diameter would require data to be corrected by about 5% to correlate with other continuum data. Nevertheless, the continuum was assumed with the aim of obtaining a consistent set of data from the numerical investigation.

In the higher Reynolds number range, care must be taken with the occurrence of compressibility effects. With a usual hot-wire anemometry probe ($D = 5$ μm) a Mach number of 0.3 is achieved in air at Re values as low as 40. In this study, larger cylinders were used at the larger Re numbers up to a diameter of 500 μm and, hence, the Mach number never exceeded 0.02. This value undoubtedly demonstrates the suitability of the incompressibility assumption in the equations employed.

A more severe restriction for the cylinder diameter was imposed by the elimination of viscous heating effects. Since the authors wanted to investigate the heat transfer from cylinders at very low temperature differences (down to 1°C), the problem of viscous heating was likely to have a strong influence if no particular care was taken in selecting the flow parameters and the cylinder diameter.

There is apparently a lack in the existing investigations of the influence of viscous dissipation on the forced convective heat transfer from a cylinder in crossflow. In the work of Sundén [46] the cylinder wall was treated as adiabatic and no influence on the Nusselt number was investigated. In order to quantify this effect, the authors computed the Nusselt number for several cases, neglecting artificially the dissipation function in equation (3). They compared the results of this reduced form of the equation with that of the complete form. The dependence of the Nu differences (normalized by Nu without viscous heating) on the values of the Eckert number is shown in Fig. 1.

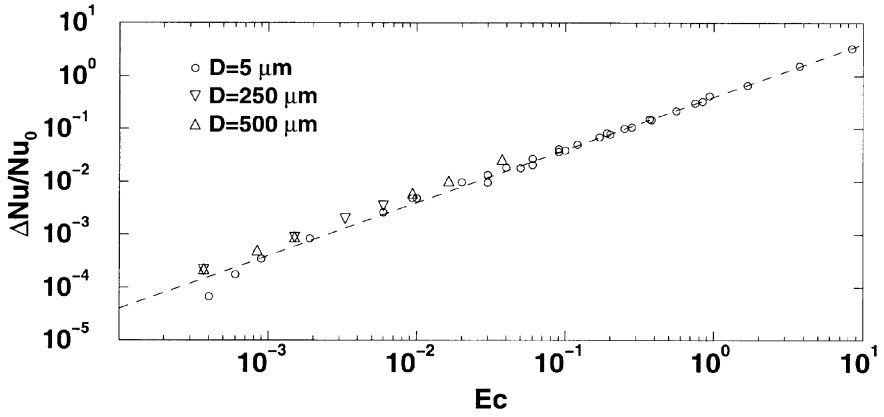

Fig. 1. Change in Nu due to viscous heating. Dashed line corresponds to equation (7).

The data shown in Fig. 1 can be summarized by the following function

$$\frac{\Delta Nu}{Nu_0} = 0.4Ec \tag{7}$$

where $\Delta Nu = Nu_0 - Nu$ and Nu_0 is the reference Nusselt number without viscous dissipation effects. Based on equation (7), the criterion $Ec < 0.01$ was adopted to ensure that the influence of viscous heating on Nu is negligible, i.e. smaller than 0.5%.

In most experimental investigations of heat transfer at very low Reynolds numbers, the occurrence of natural convection influences strongly the Nusselt number and renders investigations of pure forced convection very difficult. From equation (2), we can see that the relative gravity force is proportional to Gr/Re^2. This suggests a criterion for the onset of natural convection effects of the form

$$Re \geqslant c_1 Gr^{1/n_1} \tag{8}$$

with $n_1 = 2$. In fact, experimental investigations have found slightly different values for the exponent. Table 1 summarizes experimental results in the case of air. It should be noted that the values were obtained with fluid properties at the arithmetic mean temperature between the cylinder and free stream, also called the film temperature T_f.

All combinations of diameters and temperature differences in the present investigation satisfied equation (8) with the set of constants in Table 1 (mainly cases b and d). Besides this, in the present work pure forced convection was actually imposed by neglecting the gravity term in equation (2), ensuring the absence of any natural convection effect in the computations.

Table 1.
Values of constants in equation (8)

	c_1	n_1	Reference
(a)	1.85 $(T_f/T_\infty)^{0.76}$	2.56	Collis and Williams [12]
(b)	1.37	2.0	Oosthuizen and Madan [47]
(c)	32.6	1.97	Gebhart and Pera [48]
(d)	1.9	2.39	Hatton et al. [49]

2.3. Numerical solution method

For the spatial discretization of equations (1)–(3) a finite volume method with a colocated arrangement of the variables was employed [50]. Equations (2) and (3) were integrated over each control volume (CV), leading to a balance equation for the fluxes through the CV faces and the volumetric sources. Note that in equations (2) and (3) the fluid properties were not treated as being constant. They were calculated as functions of temperature and were updated at each new iteration. The convection and diffusion contributions to the fluxes were evaluated using a central differencing scheme, which for the convective part was implemented using the deferred correction approach.

For the pressure calculation, a pressure correction equation was used instead of equation (1) and was solved iteratively with equation (2) following the well-known SIMPLE algorithm. Convergence was achieved when the maximum sum of the normalized absolute residuals in all equations was reduced to a value less than 10^{-6}. Details about the discretization and the pressure–velocity coupling can be found in ref. [50].

For the time discretization, a slightly modified form of the Crank–Nicolson scheme was applied (see [51]), ensuring a high temporal accuracy. A few steps of the first-order fully implicit Euler scheme were used at the

beginning of a new transient computation to prevent the occurrence of small spurious velocity oscillations in the vicinity of the cylinder. In case of steady-state solutions ($Re \leqslant 45$), the stationary form of equations (2) and (3) was solved instead.

The solver for the linearized systems of equations was a parallel incomplete LU decomposition. A nonlinear multi-grid scheme was employed for convergence acceleration. For parallel computations, a block structured grid partitioning and a message passing strategy were used, as described by Durst and Schäfer [50].

In order to improve the accuracy of the numerical results without loss of efficiency and to optimize the utilization of the available computational resources, local grid refinement was employed. For the local refinement procedure the computational domain was divided into blocks and each block was discretized with a different mesh density. After refinement, each block remained fully structured, hence retaining the very efficient implementation of the code. The combination of high efficiency with high accuracy provided by the local block refinement was essential to the realization of this comprehensive investigation. For more details about the refinement procedure, see Lange [51].

2.4. Computational domain and boundary conditions

In the range of Reynolds numbers investigated in the present work, the laminar flow around a circular cylinder has three regimes: steady flow without separation ($Re \lesssim 5$), steady flow with two symmetric vortices behind the cylinder ($5 \lesssim Re \lesssim 46$) and unsteady flow with vortex shedding ($Re \gtrsim 46$). The physical characteristics of the different regimes will be summarized in Section 3. For the design of the computational domain and grid, however, it is important to consider some details at this point. Two different types of computational domains and of grids were employed: one for lower and one for larger values of Re.

For all simulations at very low Reynolds numbers ($Re < 1$), the computational domain had to be extremely large and adjusted to the actual value of Re (see Section 2.5). A domain size up to 10^6 times larger than the cylinder diameter was employed for the smallest value of Re. The region of the flow disturbed by the cylinder at low values of Re is of similar magnitude in the front and in the rear of it. For this reason, a circular domain was chosen, with an outer boundary of diameter H and an inner boundary on the cylinder surface with diameter D. The Dirichlet boundary condition (BC) was applied on the left half of the outer boundary (inflow) and Neumann BC on the right half (outflow). On the cylinder surface no-slip BC for the velocity and a constant value for the temperature were prescribed.

For Reynolds numbers larger than about five, a pair of standing vortices appear at the rear of the cylinder, demanding a finer discretization of this region. This was taken into account in the grid refinement process. The final form of the locally refined grid in the near-cylinder region was chosen after extensive numerical tests and was then employed as the core region of all numerical grids for stationary computations ($Re \lesssim 46$). At the fifth multi-grid level (actual computational grid) the surface of the cylinder was discretized with a total of 448 CVs.

For the transient flow regime at moderate Reynolds numbers ($Re \gtrsim 46$) the computational domain had to be elongated downstream in order to capture correctly the von Kármán vortex street. On the other hand, the cylinder disturbs a smaller region in the front and lateral directions compared with the other regimes. Therefore, a different type of domain was adopted for this range of Reynolds numbers. A rectangular domain with Dirichlet BC at the left (inflow), no-flux BC at the upper and lower sides and Neumann BC at the right (outflow) was used. The same BCs as in previous case were employed on the cylinder surface.

The discretization of the rectangular domain was performed by coupling an O-type grid around the cylinder with an H-type grid in the elongated part of the domain. The third level of five multi-grid levels is plotted in Fig. 2 to exemplify the discretization. The grid points were concentrated around the cylinder and in the wake region. A better view of the point distribution near the cylinder in the third grid level can be seen in the detail in Fig. 2. In the fifth level of the OH-grid, on which the present results for $Re \gtrsim 46$ were actually computed, a total of 576 CVs were used to discretize the cylinder surface.

The physical dimensions and boundary conditions investigated in the present study were similar to the case of a hot-wire anemometry probe in crossflow. The fluid considered was air at an inflow temperature of 20°C. The fluid properties were obtained from the property chart in ref. [52]. In the case of larger temperature differences, all properties were treated as temperature dependent and interpolated with a quadratic polynomial function. The cylinder diameter varied between 0.5 μm for the lower and 500 μm for the larger values of Re. The cylinder temperature was assumed to be constant with values between 21°C and 166°C. This corresponds to a range of temperature loadings (τ) from 1.003–1.5, where τ is defined as

$$\tau = \frac{T_w}{T_\infty} \tag{9}$$

both in absolute units (K). The inflow velocity was adjusted in order to cover a range of Reynolds numbers between 10^{-4} and 200.

2.5. Numerical accuracy

The locally refined grid was chosen so that it minimizes the computing time without accuracy losses. In the test

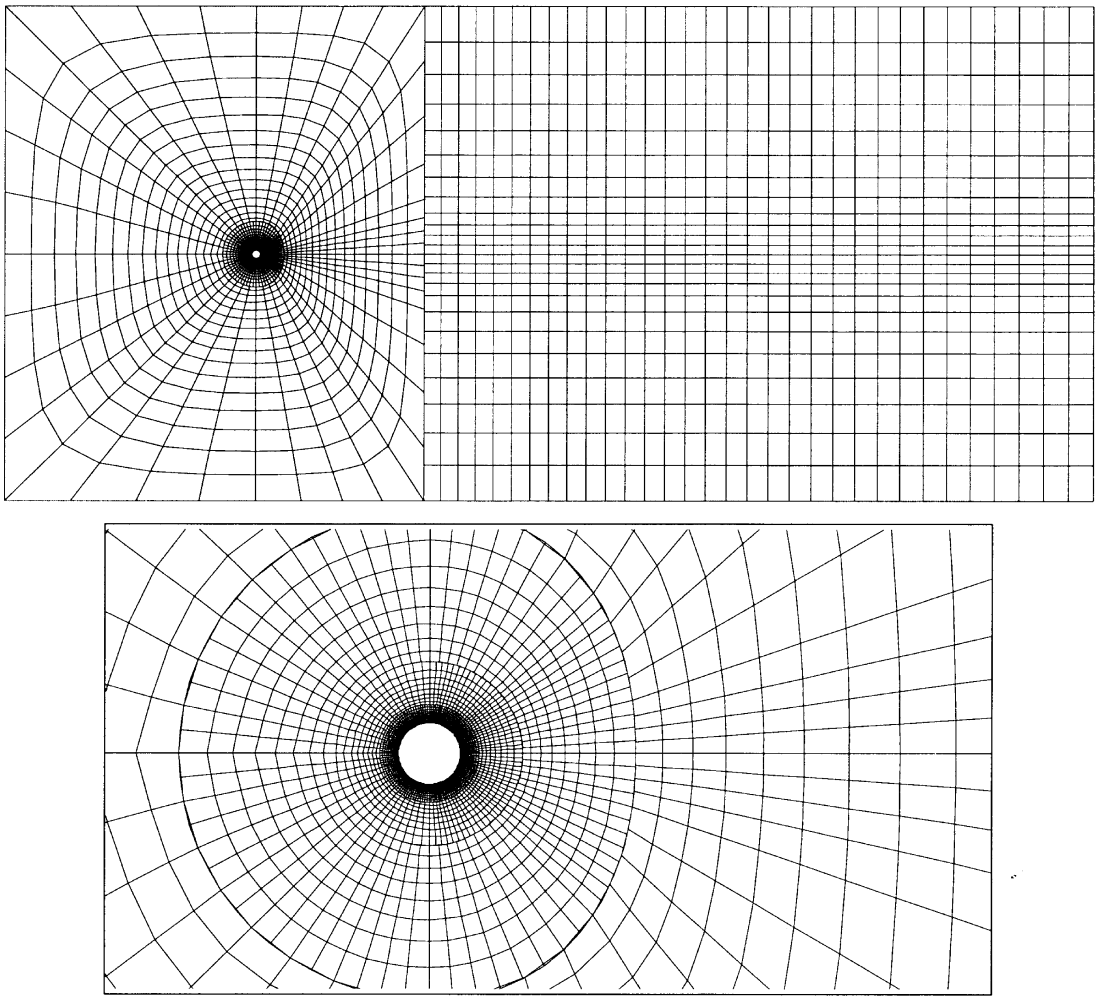

Fig. 2. Computational grid ($H/D = 60$) and zoom of the locally refined region (both at the third multi-grid level) for moderate values of Re.

comparisons between the various locally refined and a classical globally refined grid the values of integral parameters, such as the drag coefficient and Nusselt number, never showed a difference larger than 0.1%. Control computations on a further multi-grid level (CV size halved in each direction) showed a maximal change of 0.3% on these integral quantities.

In the transient computations, a time step of about 1/60 of the vortex shedding period was used. It represented a change of less than 0.1% in the mean values of Nu and C_D and in the amplitude of C_L compared with a time step equal to 1/20 of the period. This demonstrates the high accuracy of the employed Crank–Nicolson time discretization scheme.

The integral parameters, mainly C_D, showed a strong dependence on the relative size of the computational domain at very small Reynolds numbers ($Re < 1$). The reason for this is the application of conditions at the boundary, i.e. at finite distances from the cylinder, that are actually only valid at infinity. This effect was reported previously by Sucker and Brauer [34], among others.

The region of the flow influenced by the cylinder increases constantly with decreasing Reynolds numbers. The Reynolds number itself may be seen as a ratio of two characteristic lengths: the cylinder diameter D and a viscous length scale represented by v/U_∞, where v is the kinematic viscosity. This viscous length scale indicates the magnitude of the region influenced by diffusion of the cylinder momentum and it varies with Re^{-1} for a given cylinder. If the boundary of the computational

domain did not approximately accompany the expansion of the influence region at smaller Re, the error caused by the artificial boundary conditions disturbed the solution, affecting even the vicinity of the cylinder. In Fig. 3(a) the present results are plotted for different sizes of the computational domain to quantify its influence on the drag coefficient. For the sake of comparison, the analytical value obtained with matching asymptotic expansions by Kaplun [21] is also plotted.

Using the results of the largest domain ($H/D \approx 10^6$) as a reference, it was possible to estimate the minimum domain size as a function of Re for a given error level. If the same computational grids were scaled up preserving the point distribution, the minimum domain size would depend on Re^{-1}. However, this would demand the simultaneous scaling of the cylinder diameter and the corresponding adjustment of the boundary conditions far beyond the physical limits. Instead of this, the cylinder diameter was held constant and the domain size was increased by adding new grid points in the outer region. This increase in the overall number of grid points expectedly reduced the Re dependence of the minimum domain size. Indeed, for $Re < 1$ the minimum domain size was found to depend on $Re^{-0.8}$, as can be seen in Fig. 3. Figure 3(b) shows the resulting curve that gives the minimum domain necessary to reduce this source of error below 1%. This estimation results in the following criteria for the size of the computational domain in the range of $Re < 1$:

$$H/D > 320Re^{-0.8} \quad \text{for } \varepsilon_{H/D} < 1\% \tag{10}$$

$$H/D > 4000Re^{-0.8} \quad \text{for } \varepsilon_{H/D} < 0.1\% \tag{11}$$

where $\varepsilon_{H/D}$ is the error due to the domain size. The limiting line corresponding to equation (10) is shown in Fig. 3. In all stationary computations, except the lowest values of Re ($\approx 10^{-4}$), equation (11) was easily satisfied. At $Re = 10^{-4}$ the value of $\varepsilon_{H/D}$ probably did not exceed 0.5%. The authors are aware that equations (10) and (11) apply only to the specific type of boundary conditions adopted here. Nevertheless, even authors that apply some analytical solution as boundary conditions have reported a domain size dependence of the numerical results [31, 46, 53].

A domain width of $60D$ and length of $130D$ with the cylinder placed $30D$ away from the inflow boundary was used for the transient computations. The authors estimate an error due to the domain size of less than 1% for the mean quantities in most of the time-dependent calculations.

The comparison of numerical and experimental results presumes consistency with respect to the fluid properties, especially when the variation of the properties with temperature is relevant, as in the present study. If even authoritative property charts as in refs. [52] and [54] disagree in general by 1%, and in some cases up to 3%, it is a fallacy to expect a better correlation of data in comparisons with experiments. This seems to be the most relevant source of uncertainty of the present results.

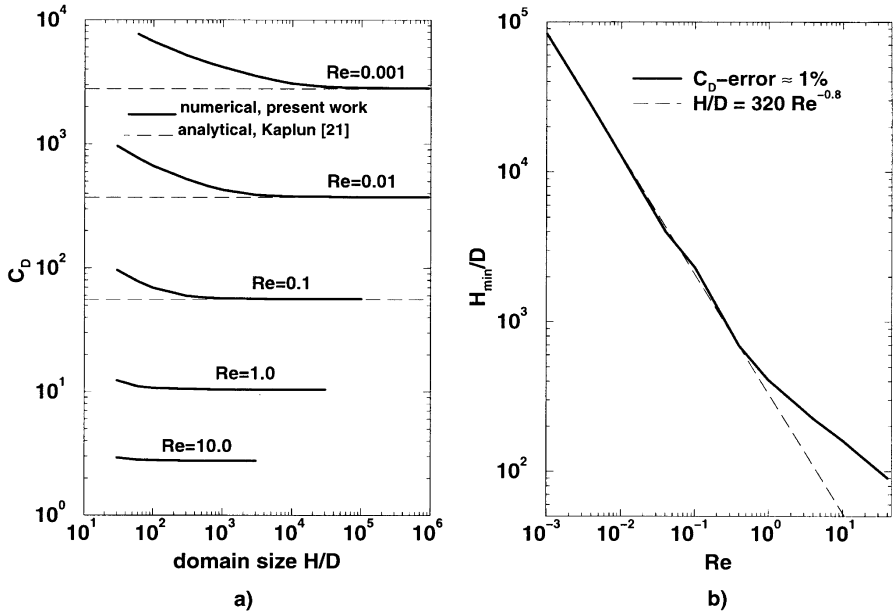

Fig. 3. Influence of the size of computational domain (a) and minimum domain size (b) for drag computations.

3. Results for constant fluid properties

3.1. Flow structure

At very low values of Re ($Re < 1$), the flow past a cylinder is characterized by the predominance of viscous transport. Owing to the increase in the viscous length scale with decreasing Re, the cylinder disturbs the flow field not only in its vicinity, but also at large distances in all directions. The numerical implications of this fact were addressed in the previous section. Up to an Re number of about five, the flow remains attached, i.e. no separation occurs at the rear of the cylinder. Besides the symmetry with respect to a horizontal plane, the streamlines are almost symmetric also with respect to a vertical plane at the cylinder axis. A detailed observation of the flow field shows, however, that the solution is actually asymmetric in the latter case. The first picture in Fig. 4 ($Re = 0.1$) is representative of this flow regime.

At Reynolds numbers greater than about five, a pair of standing vortices appears behind the cylinder. The flow is still stationary. The region of the flow influenced by the cylinder shrinks constantly in the front part, while at the rear the wake is more and more affected. This reveals the dominance of inertial forces over viscous dissipation. The size of the separated flow region increases with increasing Reynolds number, which is clearly illustrated by the two pictures for $Re = 10$ and 40 in Fig. 4.

The vortices grow until a limit at which the wake becomes unstable. At this critical value of the Reynolds number Re_c, the viscous dissipation becomes too small to ensure the stability of the flow. The vortices are shed off by the main flow, forming the well known von Kármán vortex street. The last two cases in Fig. 4 ($Re = 60$ and 200) illustrate well the characteristics of this flow regime. The increase in the vortex shedding frequency with Re can be easily recognized by means of the smaller wavelength at $Re = 200$.

A steady-state solution above the critical value Re_c is very difficult to obtain in practical cases, because it would require an extremely low level of disturbances in the experimental setup. The value of Re_c was investigated by Jackson [55] using stability analysis and was found to be $Re_c = 46.184$, which was also verified analytically by the recent work of Dušek et al. [37] using the Landau model. Norberg [56] and Nishioka and Sato [6], among others, studied the influence of the aspect ratio of the cylinder on the wake. For sufficiently large aspect ratios their experiments resulted in $Re = 47 \pm 1$. Extrapolating the amplitude of the oscillations of the lift coefficient C_L to zero the authors found a critical value of $Re_c = 45.9$.

The characteristic frequency f of the transient flow at

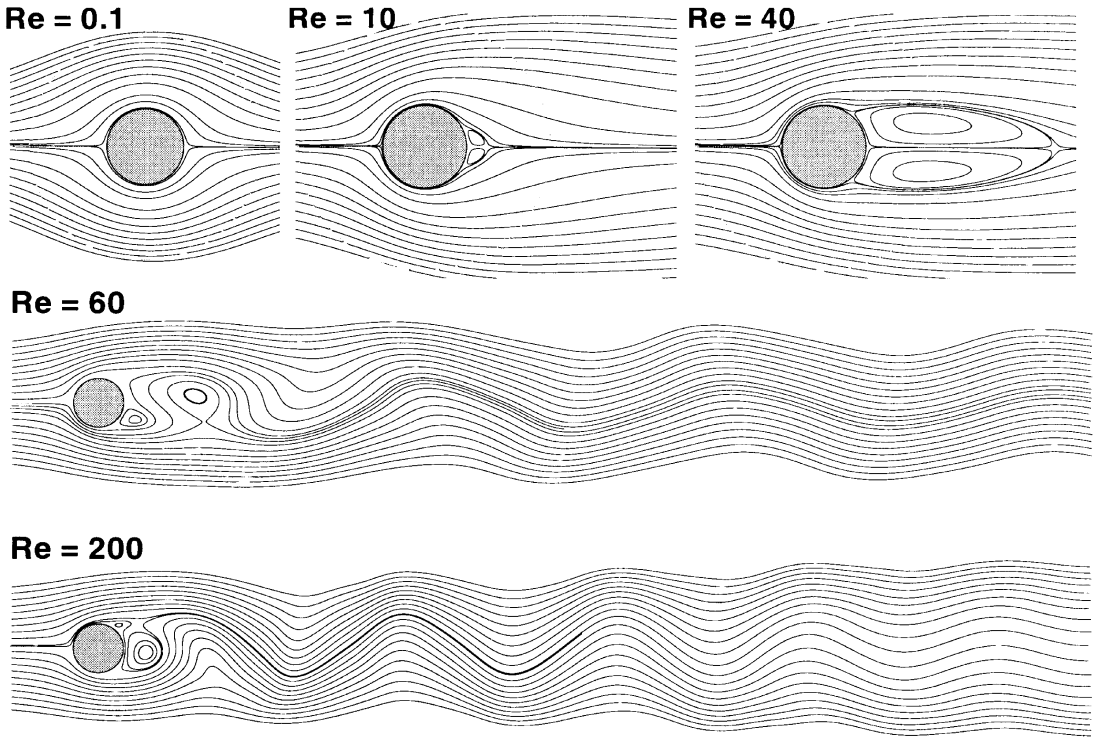

Fig. 4. Representation of the different flow regimes.

$Re > Re_c$ is expressed by the Strouhal number. Since Tritton [4] observed a discontinuity in the Strouhal curve at an Re of about 90, in contrast to the observations of Roshko [57], there was a long debate about the reason for this disagreement. The first to explain successfully this Strouhal number discontinuity was Williamson [58, 59]. He showed that this effect is caused by a transition in the shedding mode of the vortex street. Three-dimensional effects, represented by oblique vortex shedding in opposition to the two-dimensional parallel shedding, were shown to be dependent on the end conditions of the cylinder, i.e. the kind of cylinder termination in the experimental setup.

Thereafter, many others investigated the influence of end conditions, aspect ratio and background turbulence on the occurrence and angle of these oblique shedding modes (Norberg [56]; König et al. [60]; Hammache and Gharib [61]; Lee and Budwig [62]; Leweke and Provansal [63]). It is important for the present analysis to consider how far these three-dimensional effects are caused by the finite cylinder length of the experimental setup and if there is a critical value $Re_c^{3\text{-D}}$ above which two-dimensionality could no longer be assumed, even in the case of an infinite cylinder. Karniadakis and Triantafyllou [35] investigated numerically the wake stability using a spectral element technique. They found that the cylinder wake first becomes three-dimensional as a result of a secondary instability of the two-dimensional vortex street. This secondary instability appeared in their study at a Reynolds number close to 200. Using a low-dimensional Galerkin method, Noack and Eckelmann [36, 64] performed a global Floquet analysis of the stability of the wake and showed that the value of $Re_c^{3\text{-D}}$ depends on the wavelength of the three-dimensional perturbation applied to the flow. The lowest critical value was found to be $Re_c^{3\text{-D}} = 170$. Recently, a more accurate computation by Barkley and Henderson [39], using a spectral element method, showed the lowest critical value to be $Re_c^{3\text{-D}} = 188.5 \pm 1$. This value seems to be confirmed approximately by experiments such as those of Williamson [59], Leweke and Provansal [63] and Mansy et al. [65]. Therefore, it makes no sense to assume two-dimensionality of the flow past a circular cylinder for $Re > 200$. This was the reason for the choice of the upper limit of Re in the present computations.

3.2. Drag coefficient and Strouhal number

One of the most important characteristic quantities of the flow around a cylinder is the drag coefficient C_D. In the region of small Reynolds numbers the drag coefficient varies strongly with Re. The contributions of the viscous and pressure forces to the drag are very similar in this flow regime. The regime of attached flow is also the range of validity of the existing analytical solutions. A comparison of the present results for the drag coefficient with analytical solutions over the entire range of Reynolds numbers computed is shown in Fig. 5. At the lower end of the range ($Re < 10^{-4}$), only the classical Oseen/Lamb [18] solution was plotted, since all analytical solutions coincide. The excellent agreement of the numerical results with the analytical solutions is remarkable. At larger values of Re the analytical solutions tend to deviate from the computed curve. The drag coefficient expansion calculated by Tomotika and Aoi [19] shows already at $Re \approx 0.1$ a visible discrepancy of about 4%. The matched asymptotic expansion by Kaplun [21] gives a solution valid up to $Re \approx 1$. Tamada et al. [22] improved the solution of Kaplun [21] by taking the full Navier–Stokes equations in the outer region. A better solution at larger Re was also obtained by Keller and Ward [23] by computing the sum of all terms of two significant series in the matched asymptotic expansion, namely a power series in $(\ln Re)^{-1}$ and Re times a similar power series in $(\ln Re)^{-1}$. Figure 6 shows a detail on a linear scale of the comparison with the best analytical solutions, where the last two are seen to be indistinguishable from the numerical results up to $Re \approx 2$. The detailed comparison is completed with the experimental results of Tritton [4] and Huner and Hussey [7] available in this Re range.

When separation starts at the cylinder and a recirculation region develops behind it at $Re \approx 5$, the contribution of the pressure and viscous forces to the drag get out of balance. The pressure force tends to dominate the drag, while the viscous force decreases further. The accuracy of the present computations in this flow regime can only be verified by a comparison with experimental data, shown in Fig. 7. The classical results of Wieselsberger [2] (in tabular form in Prandtl et al. [66]) and Tritton [4] show a larger scatter in the data. Nishioka and Sato [6] obtained a more consistent set of data measuring the momentum thickness of the cylinder wake. Jayaweera and Mason [5] used the terminal velocity of freely falling cylinders in a viscous liquid to estimate C_D. Their data seem to be overestimated at smaller and underestimated at larger Re, in part because of lack of correction of the finite cylinder length. Huner and Hussey [7] used the same method, but corrected their data to an infinite fluid and cylinder and obtained the most accurate C_D values in the low Re range. The present results show good agreement with these data.

A comparison with other numerical results is shown in Fig. 8. The effect of a computational domain smaller than necessary is clearly recognizable in the overestimated values of Tuann and Olson [67] ($H/D = 20$) and Zhang et al. [68] ($H/D = 12$). Sucker and Brauer [34] used satisfactory domain sizes for their computations in the range $0.1 \leqslant Re \leqslant 10$ (up to $H/D = 1054$), but above this limit the domain size of $H/D = 29$ adopted was evidently insufficient. The results of Townsend [69] are based on a too coarse grid, which causes an overestimation of the drag at $Re \leqslant 1$ and an underestimation at larger Re. The

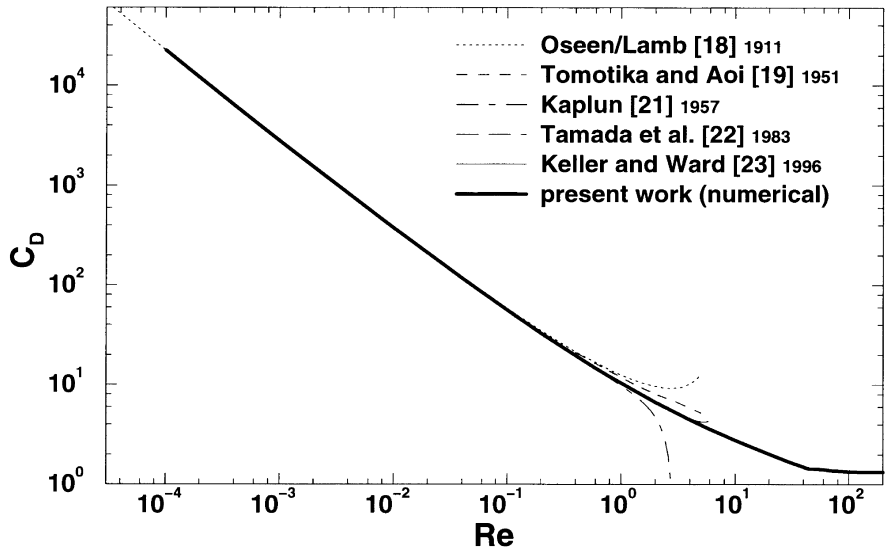

Fig. 5. Drag coefficient: comparison of numerical solution with analytical values in the entire range of *Re*.

generally underestimated values of C_D above a Reynolds number of 45 are due to stationary symmetric computations (Kawagutti and Jain [29]; Hamielec and Raal [70]; Dennis and Chang [71]; Sucker and Brauer [34]; Tuann and Olson [67]; Townsend [69]; Fornberg [72]; D'Alessio and Dennis [73]; Yang et al. [74]). This discrepancy demonstrates the unsuitability of the steady-state assumption to represent time-averaged transient flows.

Figures 7 and 8 show also a sudden change in the behavior of the computed values of C_D at $Re \approx 45$, when vortex shedding starts. This peculiarity has never been pointed out previously. The large scatter of experimental results hinders the identification of such a detail. On the other hand, stationary computations are unable to capture this change, since they just continue the curve of lower *Re* values.

In the transient flow regime, the Strouhal number constitutes an additional characteristic quantity. Figure 9 shows a comparison with other numerical results and with experimental data corresponding to pure two-dimensional parallel vortex shedding. The large values of *St* calculated by Karniadakis and Triantafyllou [77] are a consequence of a narrow domain ($H/D = 10$, as described later [35]). The data of Schumm et al. [78] are represented by their correlating curve. No reason could be devised for the smaller values of *St* measured by these authors. The accurate experimental values of Williamson [59] are represented by a curve fitting of the form

$$St = \frac{-3.3265}{Re} + 0.1816 + 1.6 \cdot 10^{-4} Re. \tag{12}$$

The present results agree very well with the latter curve.

3.3. Nusselt number

The heat transfer rate per unit area from the cylinder wall to the fluid may be described as

$$\dot{q}_w = -k_w \left.\frac{\partial T}{\partial r}\right|_w \tag{13}$$

where k_w is the thermal conductivity of the fluid at cylinder temperature and the subscript w indicates that the temperature gradient in the radial direction is evaluated at the cylinder wall. Instead of equation (13), engineers and technicians require an expression based upon measurable quantities such as

$$\dot{q}_w = h_c (T_w - T_\infty) \tag{14}$$

where h_c is the heat transfer coefficient. Nusselt [9] analyzed the heat transfer from cylinders to air in order to find a similarity condition between different flow cases. To establish this similarity, he used a normalized form of the specific heat flux called the Nusselt number[1]

$$Nu = \frac{\dot{q}_w}{\dot{q}_{ref}} = \frac{-k_w \left.\frac{\partial (T - T_w)}{\partial r}\right|_w}{k' \frac{(T_w - T_\infty)}{D}} = \frac{k_w}{k'} \left.\frac{\partial \left(\frac{T_w - T}{T_w - T_\infty}\right)}{\partial \left(\frac{r}{D}\right)}\right|_w \tag{15}$$

[1] Actually, Nusselt proposed the normalization of the heat flux from a surface dS with $Q_{ref} = k' D (T_w - T_\infty)$. Later in the same work he changed the nondimensional parameter to the form of equation (16), which corresponds to the given definition [equation (15)].

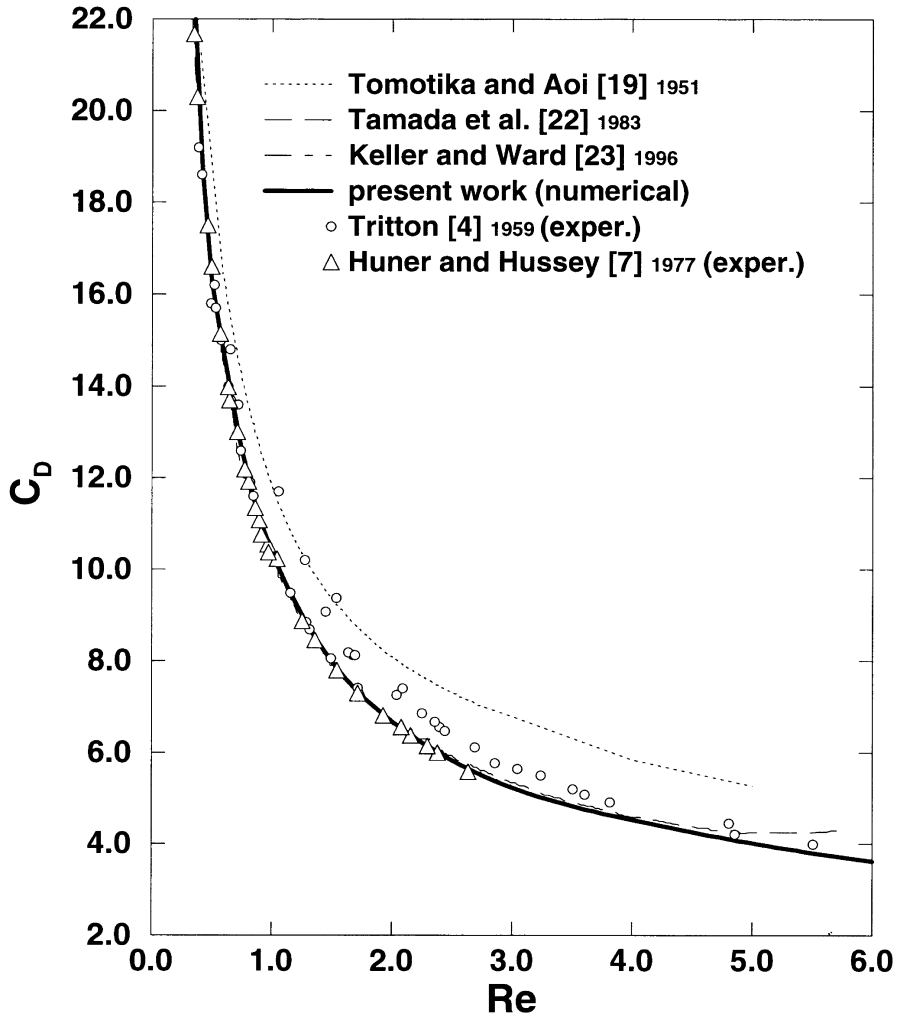

Fig. 6. Drag coefficient : detailed comparison of numerical solution with analytical and experimental values.

where $\dot{q}_{\mathrm{ref}}$ is a reference heat flux and k' the thermal conductivity at a reference temperature to be defined later. The Nusselt number can be used to obtain the actual heat flux either from equation (15) or equation (14). In the latter case, it is necessary to calculate the heat transfer coefficient from

$$Nu = \frac{h_c k'}{D}. \tag{16}$$

Usually just the mean value of the Nusselt number is needed, namely when no local effect on the cylinder surface is of particular interest. In this case, the value of Nu is averaged over the whole cylinder perimeter. In the following, we consider only the surface averaged value of Nu.

The Nu results in the present computations are presented first for the case of a very small temperature difference ($\Delta T = 1^{\circ}\mathrm{C}$). In this case the influence of temperature dependence of the properties is negligible and the problem of the definition of k' disappears.

Cole and Roshko [24] obtained an analytical expression for the Nusselt number, based on the Oseen/Lamb [18] solution for the flow. Their solution, expressed by

$$Nu = \frac{2}{\ln\dfrac{8}{Re\,Pr} - \Gamma} \tag{17}$$

is plotted in Fig. 10 together with other analytical results for the case of air ($Pr = 0.7148$). Wood [25] extended equation (17) by two terms, whereas Hieber and Gebhart [26] obtained a solution based on the method of matched asymptotic expansions. Nakai and Okazaki [80] matched

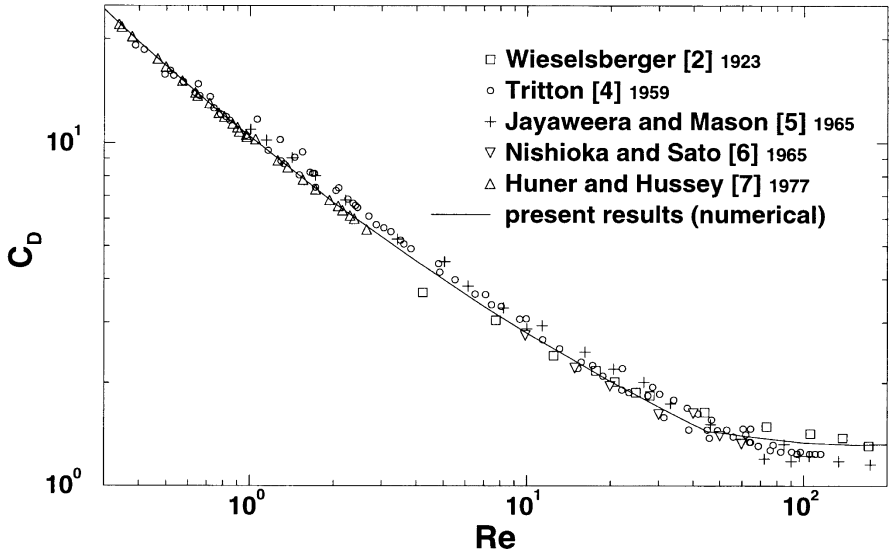

Fig. 7. Drag coefficient : comparison of the present numerical results with experimental values.

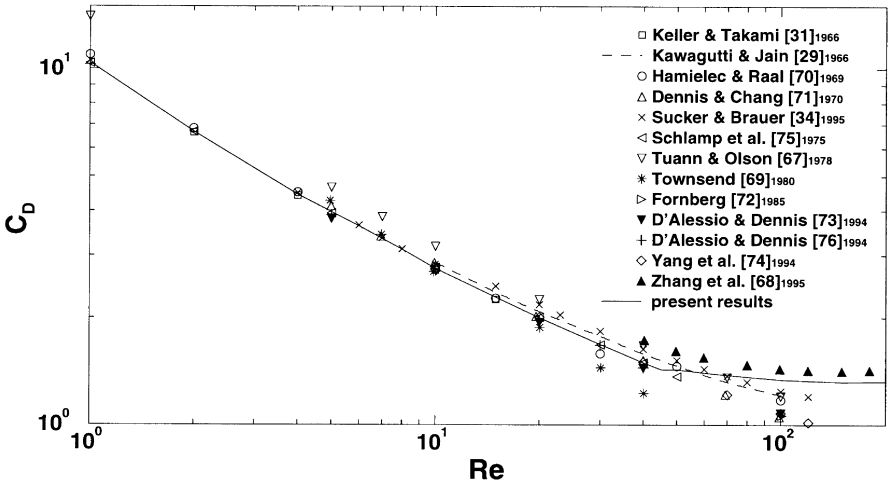

Fig. 8. Drag coefficient : comparison of the present with other numerical results.

two solutions for the temperature field, one corresponding to pure conduction in the vicinity of the cylinder and the other corresponding to a similarity solution for convection in the far field. Figure 10 shows that these analytical solutions are valid in the best cases up to $Re = 0.2$. The experimental data of Collis and Williams [12] are also shown for comparison.

Figure 11 shows a comparison with the most consistent experimental values of the Nusselt number available for forced convection in air. These data were corrected to compensate for the influence of the temperature dependence of the fluid properties and therefore are suitable for comparison with the present constant property results. The highly consistent data of Hilpert [10] were later corrected by Fand and Keswani [81], using more accurate fluid property values and compensating for the temperature difference in the same way as Collis and Williams [12]. The data of Hatton et al. [49] corresponding to their smallest cylinder ($D = 0.004$ in) were discarded, because they are inconsistently larger than other results.

Figures 10 and 11 show the excellent agreement of the

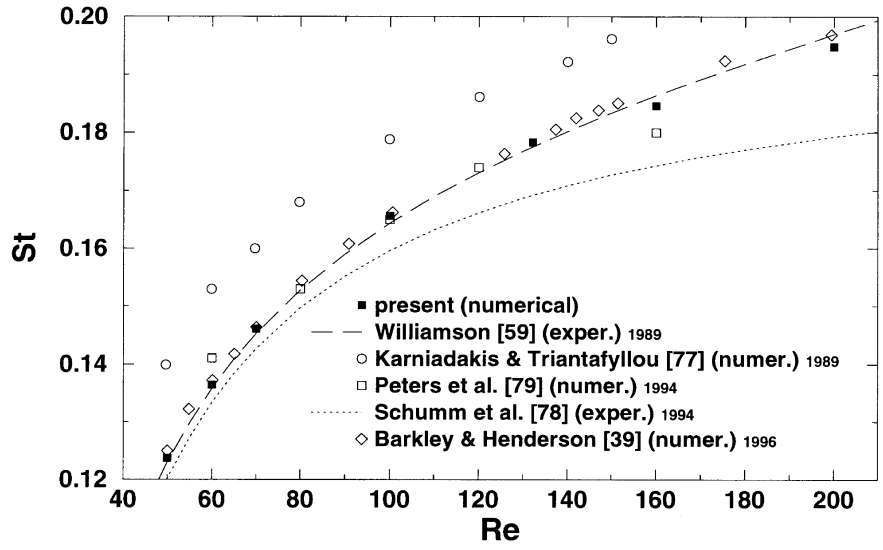

Fig. 9. Strouhal number: comparison with other numerical and experimental values.

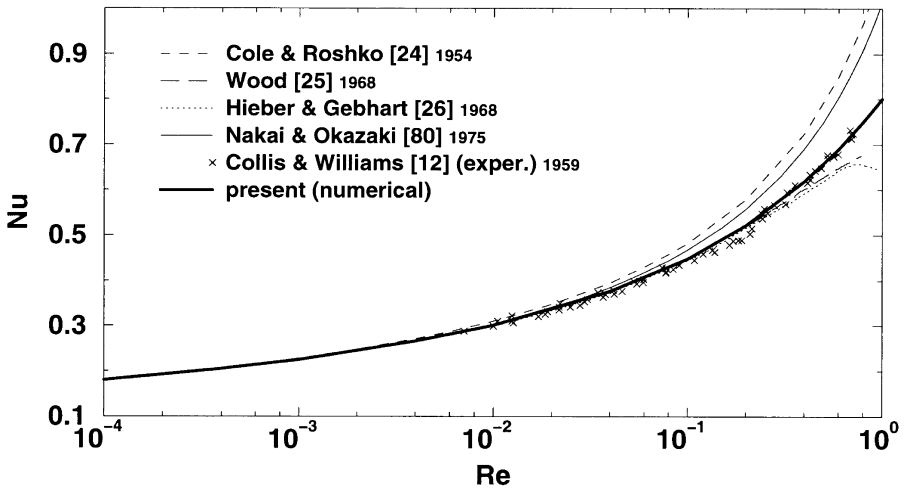

Fig. 10. Nusselt number: comparison of the present numerical results with analytical values.

present computations with both analytical (in the range of their validity) and experimental results for the Nusselt number over the complete range of Reynolds numbers computed.

Many authors have suggested functions to fit their experimental values of the Nusselt number [49, 82–84]. Collis and Williams [12] suggested two different functions, because they observed a discontinuity in the slope of the *Nu* curve at the beginning of vortex shedding. The present results also show such a discontinuity, but much weaker than in the case of the drag coefficient.

However, it is advantageous to have a single curve representing the whole range of Reynolds numbers, for example if repeated calculations of *Nu* are to be made over a large range of *Re*. For this reason, Fand and Keswani [85] interpolated the data of King [8], Hilpert [10] and Collis and Williams [12] and obtained a single correlation valid in the range $10^{-2} \leqslant Re \leqslant 2 \cdot 10^5$. The form of their function was based on physical considerations. The first term in their equation is a constant (0.184), serving as lower bound for the Nusselt number and often interpreted as the value of *Nu* in case of natural convection [83]. In the present work, only pure forced convection was considered, for which no lower bound for *Nu* exists. In other words, *Nu* vanishes when *Re* tends to zero. For this reason, a similar function was adopted

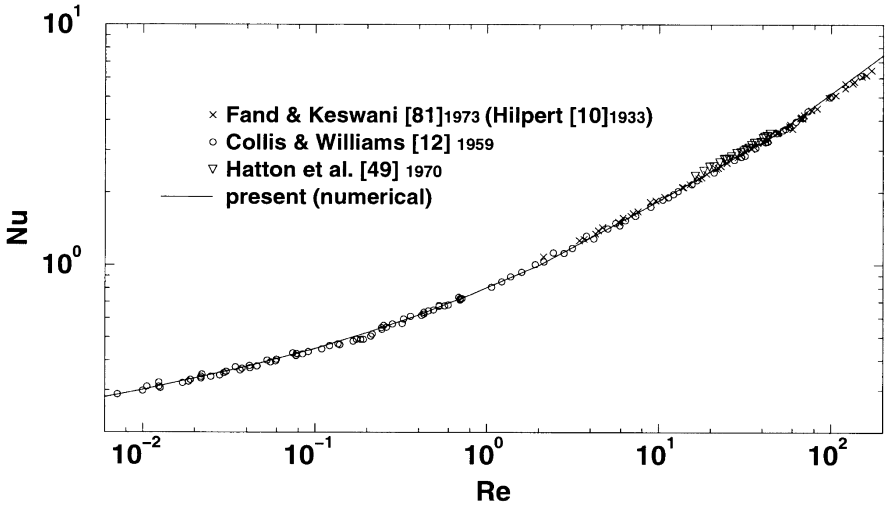

Fig. 11. Nusselt number: comparison of corrected experimental values for cylinders in air with present numerical results.

to correlate the present results, with exclusion of the constant term. The resulting equation represents the current data with an error smaller than 1.5% in the computed range of $10^{-4} \leqslant Re \leqslant 200$

$$Nu = 0.082Re^{0.5} + 0.734Re^{\chi} \tag{18}$$

where $\chi = 0.05 + 0.226Re^{0.085}$.

Besides the advantages of having a single function of Nu for the entire range, there is the obvious disadvantage that equation (18) smooths the small change in the slope at $Re \approx 45$. Hence, to prevent the suppression of details, the curves in Figs 10–12 were plotted by the connection of the actual numerical results, instead of using curve fitting, as in equations (18).

As already mentioned in the Introduction, there are only a few publications on the numerical solution of the present problem. Dennis et al. [41] discretized the stream function-vorticity equations using series truncation and finite difference methods. They applied the solution of Cole and Roshko [24] as boundary condition [equation (17)], which probably caused the overestimation of Nu at Re larger than 10. Sucker and Brauer [42] obtained slightly overestimated results in all their computations, except at $Re = 100$ and 120, where the effect caused by the stationary computation compensated the overestimation. Both numerical results are presented in Fig. 12.

4. Influence of temperature-dependent properties

The influence of variable fluid properties on the nondimensional parameters will be addressed in the following. In addition, some special formulations and corrections that compensate for this influence are evaluated and discussed. In order to introduce these different formulations better, the analysis starts with the Nusselt number.

4.1. Nusselt number

We recall that the main goal of the Nusselt number is to serve as a similarity condition to identify the independent parameters governing the convective heat transfer. In the case of constant fluid properties and negligible natural convection and dissipation effects, equations (2) and (3) show that the Nusselt number depends only on two parameters, namely the Reynolds and Prandtl numbers. However, if the temperature differences are not small, the variations of the fluid properties have to be taken into account. As a consequence, Nusselt [9] showed that the convective heat transfer depends on an additional parameter, the temperature loading τ, defined in equation (9). This arises from equations (2) and (3), when the nondimensional properties are expressed in powers of the temperature ratio:

$$\mu^* = \frac{\mu}{\mu_\infty} = \left(\frac{T}{T_\infty}\right)^m, \quad k^* = \frac{k}{k_\infty} = \left(\frac{T}{T_\infty}\right)^n.$$

Equations (2) and (3) show how the problem depends on the variation of the fluid properties. Consequently, the Nusselt number will also depend on the temperature loading and, for each value of τ, a new Nu curve will be obtained.

Attempting to compensate for the temperature dependence of the fluid properties, Nusselt [9] proposed the use of mean values of these properties integrated between wall and free stream temperatures for the calculation of

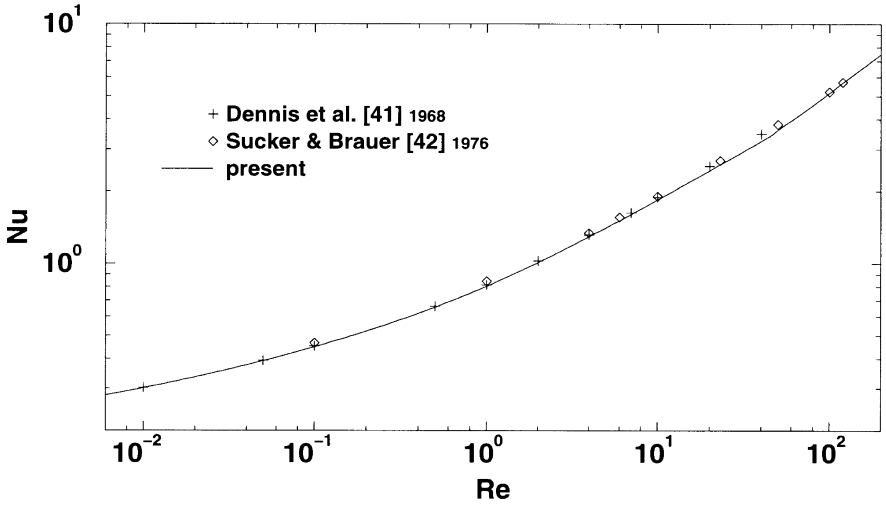

Fig. 12. Nusselt number: comparison of present with other numerical results for cylinders in air.

the nondimensional parameters. He hoped in this way to circumvent approximately the explicit dependence on the temperature loading. In other words, the use of integrated mean properties would allow the correlation of data with different temperature loadings into a single curve.

Following Nusselt's suggestion, Hilpert [10] and Schmidt and Wenner [86] used the integrated mean values of the properties to present their data. Alternatively, many authors used the properties at the arithmetic mean temperature, also called the film temperature T_f, as a simple approximation to the integrated mean value. Other authors, such as McAdams [11] and Douglas and Churchill [87], mixed the density at the free stream temperature with all other properties calculated at the film temperature, trying to group their scattered results on a single curve. Using an asymptotic expansion for very small temperature loadings, Gersten and Herwig [88] tried to find analytically the optimal reference temperature for the properties in the case of a laminar boundary layer flow and small heat fluxes. They obtained a complex expression that yields for gases a value near the film temperature. Figure 13 illustrates the effect of the use of film temperature for all properties. Results were computed for various values of temperature loading in the range $1.003 \leqslant \tau \leqslant 1.5$, corresponding to temperature differences up to 146.5°C. It can easily be recognized that there remains a systematic difference between the curves.

Some authors attempted to group their data correcting the Nusselt number by means of a ratio of some or all properties involved. Wehle and Brandt [89] investigated the influence of the temperature dependence of the fluid properties using a semi-analytical solution of the flow over a flat plate evaluated in a variety of cases. They concluded that Nu_∞, i.e. the Nusselt number calculated with properties at inflow temperature, should be corrected by a combination of ratios of μ, k, ρ and c_P.

The most comprehensive analytical investigation on the Nu correction by property ratio was the already cited work of Gersten and Herwig [88], together with the subsequent application of the same method by Herwig and Wickern [90]. All properties were expanded as a Taylor series about a reference state (the free stream temperature) with asymptotic small heat transfer rates. The truncated series were applied to solvable boundary layer problems, allowing for the determination of exponents of the property ratio corrections. Herwig [91] then combined the corrections for the flow over a flat plate and for the flow near a stagnation point, aiming to find a correction valid in the case of laminar flow around bluff bodies. However, all these analytical solutions proved to be inappropriate to the present case of a more complex flow and larger temperature loadings. The corrections are smaller than 2% at $\tau = 1.50$, causing almost no change to the results calculated at T_∞, the case with the largest deviations between the curves.

Another group of authors prefer to combine the use of mean property values with an additional correction based on a temperature ratio in order to achieve a better correlation of the data. In his very consistent set of measurements, Hilpert [10] already verified the need for a further correction to compensate for the effect of the temperature loading. He proposed the use of $\tau^{0.25}$ as a factor to correct Re_m in his functions for Nu_m, both calculated with the integral mean value of the properties.

Later, Collis and Williams [12] published one of the best experimental investigations on the effect of tem-

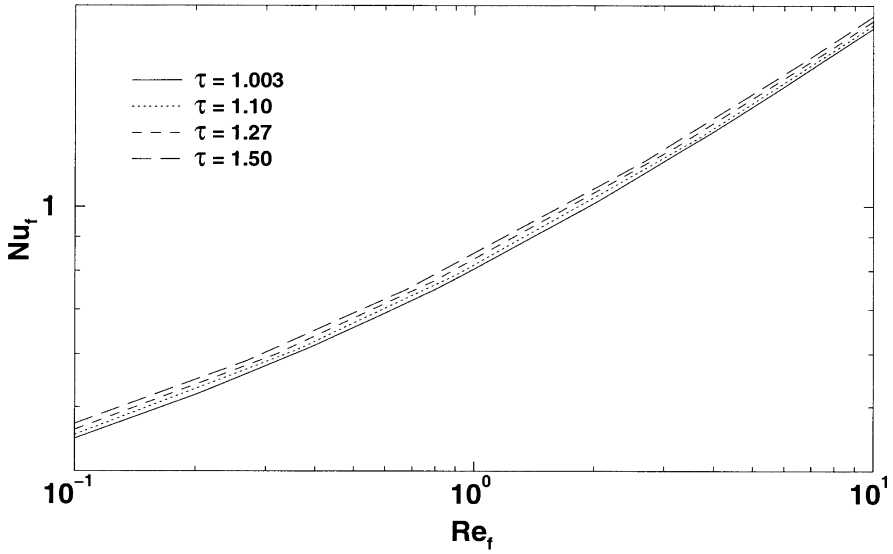

Fig. 13. Nusselt number: calculated values at different temperature loadings with properties at the film temperature.

perature loading and proposed the ratio of the film temperature T_f to the free stream temperature T_∞ as a coefficient to correct Nu_f, the Nusselt number based on properties at the film temperature. They correlated their experimental data in the range $0.02 \leqslant Re_f \leqslant 140$ with equations of the form:

$$Nu_f\left(\frac{T_f}{T_\infty}\right)^{-0.17} = f(Re_f) \tag{19}$$

Hatton et al. [49] also correlated their data in the range $0.6 \leqslant Re_f \leqslant 40$ using the same ratio but with a slightly different exponent.

More recently, the correction factor of Collis and Williams [12] [equation (19)] was used by Fand and Keswani [85] to derive a single function correlating the data of many authors in a very large range of Reynolds numbers ($10^{-2} \leqslant Re_f \leqslant 2\cdot 10^5$). In the previous section a similar equation was derived to fit the current results for the case of constant properties [equation (18)]. By applying the correction factor of Collis and Williams [12] and consistently calculating Re and Nu at the film temperature, the same equation was found to correlate the complete set of present results. Its final form is given by

$$Nu_f\left(\frac{T_f}{T_\infty}\right)^{-0.17} = 0.082Re_f^{0.5} + 0.734Re_f^{\chi} \tag{20}$$

where $\chi = 0.05 + 0.226Re_f^{0.085}$.

Equation (20) was verified within the limits $10^{-4} \leqslant Re \leqslant 200$ and $1.003 \leqslant \tau \leqslant 1.5$, but it is expected to be valid also for larger values of τ. When the present numerical results were plotted with the Nu correction of Collis and Williams [12], the curves turned out to be virtually indistinguishable over the whole range of Re. For a comparison with experiments Fig. 11 should suffice, since the experimental data had temperature loadings varying between 1 and 2 and all the present results coincide with the plotted curve.

Although equation (20) correlate successfully Nu results for air with different temperature loadings, the empirical correction proposed by Collis and Williams [12] lacks the generality expected from a nondimensional relationship. The same limitation affects all corrections described. An ideal nondimensional relationship should not depend on the kind of fluid involved. In the authors' opinion, the problem has been approached in an inappropriate manner. To obtain a single universal curve of the Nusselt number there must be a suitable reference heat flux that normalizes equation (15) without the need for further corrections.

From equation (15) it seems obvious that, for a reasonable definition of the reference heat flux at the cylinder wall, the appropriate temperature for the thermal conductivity is the wall temperature ($k' = k_w$). Such a normalization heat flux takes the property changes with the temperature fully into account and is expected to correlate better the results for different temperature loadings without further correction. For consistency the Reynolds number (and the Prandtl number in the case of liquids) should be also evaluated at the cylinder temperature. This is equivalent to considering the fluid properties as constant at the cylinder temperature value. Figure 14 shows the present results with the fluid properties at the cylinder temperature. A very good correlation of the data

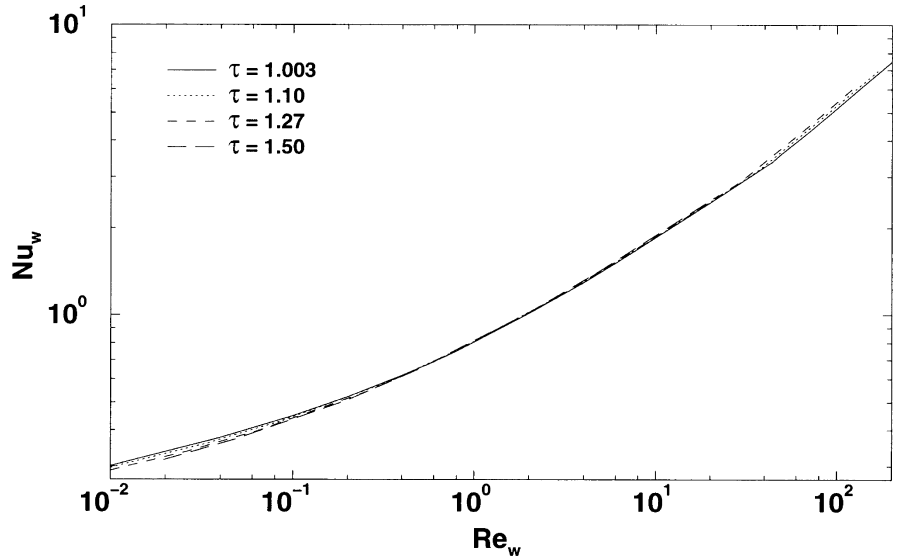

Fig. 14. Nusselt number: calculated results at different temperature loadings with properties at cylinder temperature.

is verified in the Re_∞ range between 0.3 and 45 (steady-state limit). However, in the region of very small Re_∞ numbers larger values of τ tend to produce smaller values of Nu_w. The opposite tendency of Nu_w is verified at larger Re_∞ corresponding to the vortex shedding regime.

The idea behind the use of properties at the cylinder temperature is an assumption of a linear dependence between the temperature gradient at the cylinder wall and the reference temperature gradient, i.e.

$$Nu_w = \frac{-\left.\frac{\partial(T-T_w)}{\partial r}\right|_w}{\frac{(T_w-T_\infty)}{D}} \approx \text{const} \quad \text{for a given } Re_w. \tag{21}$$

This assumption is evidently not applicable at very small values of Re and in the vortex shedding regime. This means that the search for an ideal normalization of the Nusselt number has to be continued. In spite of this, the proposed representation of the Nusselt number remains useful, since e.g. in the majority of the applications of hot-wire anemometry the Reynolds number based on the wire diameter is within the validity range ($0.3 \leqslant Re_\infty \leqslant 45$).

4.2. Drag coefficient and Strouhal number

The influence of the fluid property variations with temperature on the drag coefficient of circular cylinders in the flow of air is shown in Fig. 15. Calculating C_D and Re in the usual way with properties ρ and μ at free stream temperature, the drag coefficient increases with the temperature loading. The increase in the drag is relatively smaller at larger values of Re, where the pressure forces tend to dominate.

Following the idea developed for the Nusselt number, the computed drag coefficient values are plotted against the Reynolds number with properties evaluated at cylinder temperature. Figure 16 shows the resulting curves. Up to $Re \approx 0.1$ the curves coincide very well. At larger Re again there is an increase in the drag coefficient for larger values of τ. At $Re > 10$ the distance between the curves is even larger than with properties at the free stream temperature. This means that at very small Re, when the viscous and pressure forces are well balanced, the drag experienced by a heated cylinder is the same as in the isothermal flow case, in which all the fluid is at the cylinder temperature.

No clear tendency could be recognized in the Strouhal number with increase in the cylinder temperature. Slightly smaller St values ($\sim 0.5\%$) below an Re of 100 and slightly larger values ($\sim 1\%$) above this limit can be seen in Fig. 17. In the scope of the present investigation, no reason could be found for this behavior. The vortex shedding frequency is apparently determined by the pressure characteristics of the flow around the cylinder and almost not influenced by the cylinder temperature.

5. Conclusions

An extensive and detailed numerical investigation of the two-dimensional laminar flow of air around a heated circular cylinder has been carried out. A very efficient finite volume code employing multi-grid and local grid

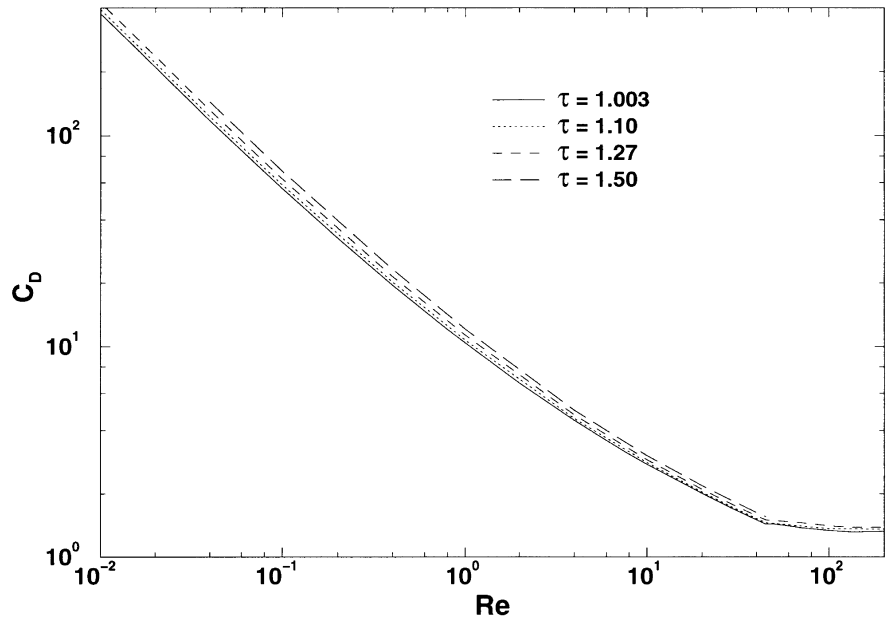

Fig. 15. Drag coefficient : calculated results at different temperature loadings with properties at T_∞.

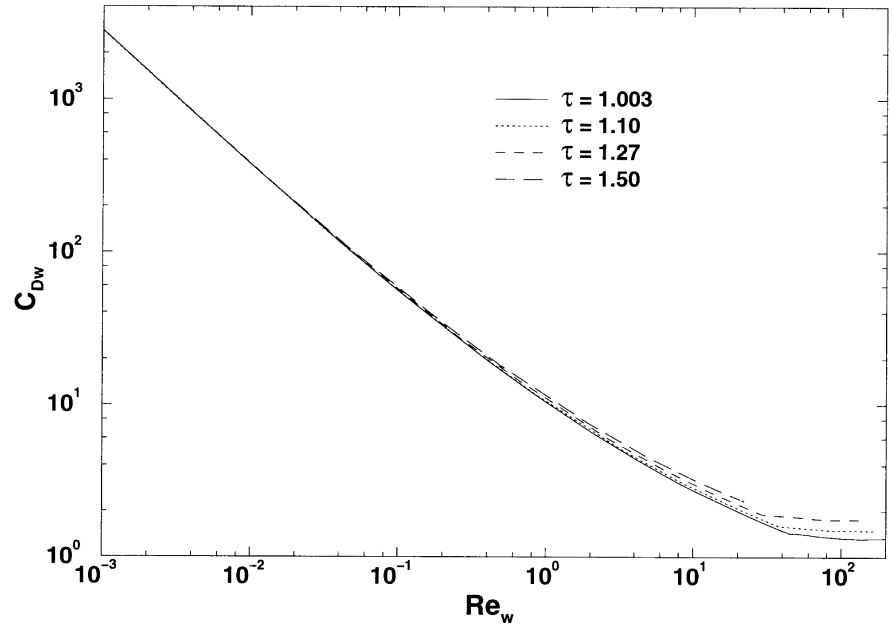

Fig. 16. Drag coefficient : calculated results at different temperature loadings with properties at the cylinder temperature.

refinement techniques led to highly accurate results for the drag coefficient and Strouhal and Nusselt numbers.

In the Reynolds number range 10^{-4}–200 the characteristics of the different flow regimes were described. The behavior of the relevant parameters C_D, St and Nu with the Re was investigated in detail first for the case of a small temperature loading ($\tau = 1.003$), when the fluid properties may be treated as constant. Good agreement was found in comparison with available analytical solutions and also with experimental data in the range of their validity. The highly accurate results of the present study revealed a sudden change in the drag coefficient

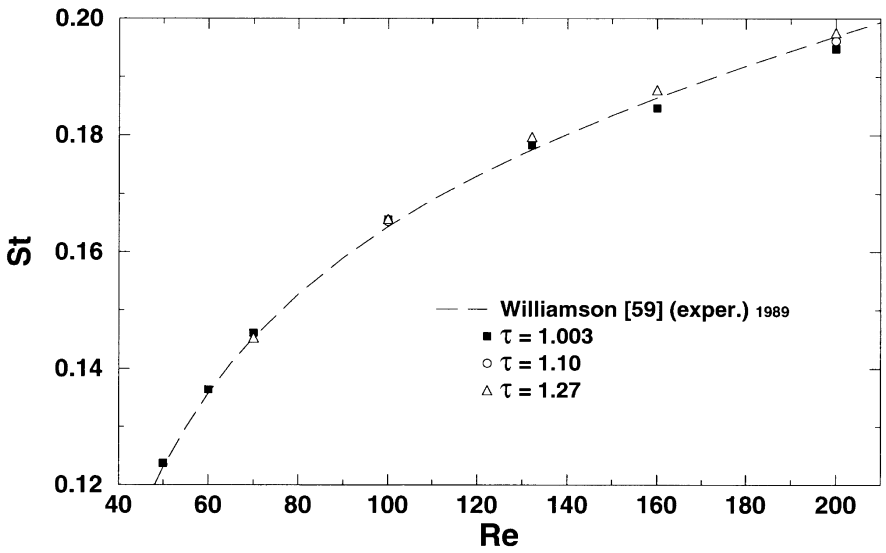

Fig. 17. Strouhal number: calculated results at different temperature loadings compared with experimental data (properties at T_∞).

curve at the beginning of the vortex shedding regime. This effect has not been reported in any previous experimental or numerical investigation. The critical Reynolds number where vortex shedding starts was determined to be $Re_c = 45.9$.

The study was completed with the investigation of the influence of the temperature-dependent fluid properties on the nondimensional parameters. The temperature loading was varied between 1.003 and 1.5 and the resultant effect on the C_D, St and Nu was analyzed. Various types of Nu formulations and corrections proposed in the literature for the correlation of data at different temperature loadings were compared. Finally, a new formulation was proposed, which correlates well the computed Nu results in the range $0.3 \leqslant Re_\infty \leqslant 45$ without any empirical correction, evaluating the Nusselt and Reynolds numbers with properties at the cylinder temperature. A good coincidence of the C_D curves was also obtained by this method in the lower Re number range ($Re < 0.1$). However, the goal of finding an ideal normalization that suppresses completely the influence of the variation of the fluid properties will be the subject of further investigations.

Acknowledgements

The authors express their thanks to Priv.-Doz. Dr H. Raszillier for the helpful discussions and suggestions. This work was supported by a fellowship from the German Academic Exchange Program (DAAD) for C. F. Lange and by a research grant from the Bavarian Consortium for High Performance Scientific Computing (FORTWIHR), which are gratefully acknowledged.

References

[1] Schlichting H, Gersten K. Grenzschicht-Theorie. 9th ed. Berlin: Springer, 1997.
[2] Wieselsberger C. Neuere Feststellungen über die Gesetze des Flüssigkeits- und Luftwiderstandes. Phys Z 1921;22(11):321–8.
[3] Finn RK. Determination of the drag on a cylinder at a low Reynolds numbers. J Appl Phys 1953;24(6):771–3.
[4] Tritton DJ. Experiments on the flow past a circular cylinder at low Reynolds numbers. J Fluid Mech 1959;6:547–67.
[5] Jayaweera KOLF, Mason BJ. The behavior of freely falling cylinders and cones in a viscous fluid. J Fluid Mech 1965;22(4):709–20.
[6] Nishioka M, Sato H. Measurements of velocity distributions in the wake of a circular cylinder at low Reynolds numbers. J Fluid Mech 1974;65:97–112.
[7] Huner B, Hussey RG. Cylinder drag at low Reynolds number. Phys Fluids 1977;20(8):1211–8.
[8] King LV. On the convection of heat from small cylinders in a stream of fluid: determination of the convection constants of small platinum wires with applications to hot-wire anemometry. Phil Trans R Soc London A 1914;214:373–432.
[9] Nusselt W. Das Grundgesetz des Wärmeüberganges. Gesund.-Ing 1915;38(42):477–82.
[10] Hilpert R. Wärmeabgabe von geheizten Drähten und Rohren im Luftstrom. Forsch G Ing 1933;4(5):215–24.
[11] McAdams WH. Heat Transmission. 3rd ed. Kogakusha, Tokyo: McGraw-Hill, 1954.

[12] Collis DC, Williams MJ. Two-dimensional convection from heated wires at low Reynolds numbers. J Fluid Mech 1959;6:357–84.
[13] Kast W, Krischer O. Die wissenschaftlichen Grundlagen der Trocknungstechnik. 3rd ed. Berlin : Springer, 1978.
[14] Merker, GP. Konvektive Wärmeübertragung. Berlin : Springer, 1987.
[15] Williamson CHK. Vortex dynamics in the cylinder wake. Annu Rev Fluid Mech 1996;28:477–539.
[16] Stokes GG. On the effect of the internal friction of fluids on the motion of pendulums. Trans Camb Phil Soc 1851;9(2):8–106.
[17] Oseen CW. Über die Stokes'sche Formel und über eine verwandte Aufgabe in der Hydrodynamik. Ark Mat Astron Fys 1910;6(29).
[18] Lamb H. On the uniform motion of a sphere through a viscous fluid. Phil Mag 1911;21:112–21.
[19] Tomotika S, Aoi T. An expansion formula for the drag on a circular cylinder moving through a viscous fluid at small Reynolds numbers. Quart J Mech Appl Math 1951;4(4):401–5.
[20] Proudman I, Pearson JR. Expansions at small Reynolds numbers for the flow past a sphere and a circular cylinder. J Fluid Mech 1957;2:237–62.
[21] Kaplun S. Low Reynolds number flow past a circular cylinder. J Math Mech 1957;6(5):595–603.
[22] Tamada K, Miura H, Miyagi T. Low-Reynolds-number flow past a cylindrical body. J Fluid Mech 1983;132:445–55.
[23] Keller JB, Ward MJ. Asymptotics beyond all orders for a low Reynolds number flow. J Eng Math 1996;30:253–65.
[24] Cole J, Roshko A. Heat transfer from wires at Reynolds numbers in the Oseen range. Proc Heat Transfer and Fluid Mech Inst 1954;6:357–84. Berkeley, CA : University of California.
[25] Wood WW. Calculation for anemometry with fine hot wires. J Fluid Mech 1968;32(1):9–19.
[26] Hieber CA, Gebhart B. Low Reynolds number heat transfer from a circular cylinder. J Fluid Mech 1968;32(1):21–8.
[27] Thom A. The flow past circular cylinders at low speed. Proc Roy Soc London A 1933;141:651–69.
[28] Kawaguti M. Numerical solution of the Navier–Stokes equations for the flow around a circular cylinder at Reynolds number 40. J Phys Soc Japan 1953;8(6):747–57.
[29] Kawaguti M, Jain P. Numerical study of a viscous fluid flow past a circular cylinder. J Phys Soc Japan 1966;21(10):2055–62.
[30] Ingham DB. Note on the numerical solution for unsteady viscous flow past a circular cylinder. J Fluid Mech 1968;31(4):815–8.
[31] Keller HB, Takami H. Numerical studies of steady viscous flow about cylinders. In: Greenspan D, editor. Numerical Solutions of Nonlinear Differential Equations. New York : Wiley, 1966. pp. 115–40.
[32] Fromm J, Harlow H. Numerical solution of the problem of vortex street development. Phys Fluids 1963;6(7):975–82.
[33] Thoman DC, Szewczyk AA. Time-dependent viscous flow over a circular cylinder. Phys Fluids Suppl II 1969;12:76–86.
[34] Sucker D, Brauer H. Fluiddynamik bei quer angeströmten Zylindern. Wärme-Stoffübertragung 1975;8:149–58.
[35] Karniadakis GE, Triantafyllou GS. Three-dimensional dynamics and transition to turbulence in the wake of bluff objects. J Fluid Mech 1992;238:1–30.
[36] Noack BR, Eckelmann H. A global stability analysis of the steady and periodic cylinder wake. J Fluid Mech 1994;270:297–330.
[37] Dušek J, Le Gal P, Fraunié P. A numerical and theoretical study of the first Hopf bifurcation in a cylinder wake. J Fluid Mech 1994;264:59–80.
[38] Henderson RD, Barkley D. Secondary instability in the wake of a circular cylinder. Phys Fluids 1996;8(6):1683–85.
[39] Barkley D, Henderson RD. Three-dimensional Floquet stability analysis of the wake of a circular cylinder. J Fluid Mech 1996;322:215–41.
[40] Dauchy C, Dušek J, Fraunié P. Primary and secondary instabilities in the wake of a cylinder with free ends. J Fluid Mech 1997;332:295–339.
[41] Dennis SCR, Hudson JD, Smith N. Steady laminar forced convection from a circular cylinder at low Reynolds numbers. Phys Fluids 1968;11(5):933–40.
[42] Sucker D, Brauer H. Stationärer Stoff- und Wärmeübergang an stationär quer angeströmten Zylindern. Wärme- Stoffübertragung, 1976;9:1–12.
[43] Ho CJ, Wu MS, Jou JB. Analysis of buoyancy-aided convection heat transfer from a horizontal cylinder in a vertical duct at low Reynolds number. Wärme-Stoffübertragung, 1990;25:337–43.
[44] Sundén B. Influence of buoyancy forces and thermal conductivity on flow field and heat transfer of circular cylinder at small Reynolds number. Int J Heat Mass Transfer 1983; 26(9):1329–38.
[45] Hatanaka K, Kawahara M. A numerical study of vortex shedding around a heated/cooled cylinder by the three-step Taylor–Galerkin method. Int J Num Methods Fluids 1995;21:857–67.
[46] Sundén B. Viscous heating in forced convective heat transfer across a circular cylinder at low Reynolds number. Int J Num Methods Eng 1992;35:729–36.
[47] Oosthuizen PH, Madan S. The effect of flow direction on combined convective heat transfer from cylinders to air. J Heat Transf ASME 1971;93:240–42.
[48] Gebhart B, Pera L. Mixed convection from long horizontal cylinders. J Fluid Mech 1970;45(1):49–64.
[49] Hatton AP, James DD, Swire HW. Combined forced and natural convection with low-speed air flow over horizontal cylinders. J Fluid Mech 1970;42(1):17–31.
[50] Durst F, Schäfer M. A parallel blockstructured multigrid method for the prediction of incompressible flows. Int J Num Methods Fluids 1996;22:549–65.
[51] Lange CF. Numerical predictions of heat and momentum transfer from a cylinder in crossflow with implications to hot-wire anemometry. Ph.D. thesis, Lehrstuhl für Strömungsmechanik, Friedrich-Alexander-Universtät Erlangen-Nürnberg, Erlangen, 1997.
[52] Verein Deutscher Ingenieure. VDI-Wärmeatlas. 6th ed. Düsseldorf: VDI, 1991.
[53] Lucchi CW. Finite element approach to the viscous incompressible flow around a circular cylinder. AIAA J 1977;15(6):887–9.
[54] Hewitt GF, editor. Hemisphere Handbook of Heat Exchanger Design. New York : Hemisphere, 1990.

[55] Jackson CP. A finite-element study of the onset of vortex shedding in flow past variously shaped bodies. J Fluid Mech 1987;182:23–45.
[56] Norberg C. An experimental investigation of the flow around a circular cylinder : influence of aspect ratio. Comput Fluids 1973;1:59–71.
[57] Roshko A. On the drag and shedding frequency of two-dimensional bluff bodies. Technical Note 3169, Washington : NACA, 1954.
[58] Williamson CHK. Defining a universal and continuous Strouhal–Reynolds number relationship for the laminar vortex shedding of a circular cylinder. Phys Fluids 1988;31(10):2742–4.
[59] Willimason CHK. Oblique and parallel modes of vortex shedding in the wake of a circular cylinder at low Reynolds numbers. J Fluid Mech 1989;206:579–627.
[60] König M, Eisenlohr H, Eckelmann H. The fine structure in the Stouhal–Reynolds number relationship of the laminar wake of a circular cylinder. Phys Fluids A 1990;2(9):1607–14.
[61] Hammache M, Gharib M. An experimental study of the parallel and oblique vortex shedding from circular cylinders. J Fluid Mech 1991;232:567–90.
[62] Lee T, Budwig R. A study of the effect of aspect ratio on vortex shedding behind circular cylinders. Phys Fluids A 1991;3(2):309–15.
[63] Leweke T, Provansal M. The flow behind rings : bluff body wakes without end effects. J Fluid Mech 1995;288:265–310.
[64] Noack BR, Eckelmann H. A low-dimensional Galerkin method for the three-dimensional flow around a circular cylinder. Phys Fluids 1994;6(1):124–43.
[65] Mansy H, Yang P-M, Williams DR. Quantitative measurements of three-dimensional structures in the wake of a circular cylinder. J Fluid Mech 1994;270:277–96.
[66] Prandtl L, Wieselsberger C, Betz A. Ergebnisse der aerodynamischen Versuchsanstalt zu Göttingen, vol. II. Munich : R Oldenburg Verlag, 1923.
[67] Tuann S, Olson MD. Numerical studies of the flow around a circular cylinder by a finite element method. Comput Fluids 1978;6:219–40.
[68] Zhang H.-Q, Fey U, Noak BR, König M, Eckelmann H. On the transition of the cylinder wake. Phys Fluids 1995;7(4):779–94.
[69] Townsend P. A numerical simulation of Newtonian and visco-elastic flow past stationary and rotating cylinders. J Non-Newt Fluid Mech 1980;6:219–43.
[70] Hamielec AE, Raal JD. Numerical studies of viscous flow and around circular cylinders. Phys Fluids 1969;12(1):11–17.
[71] Dennis SCR, Chang Gau-Zu. Numerical solutions for steady flow past a circular cylinder at Reynolds numbers up to 100. J Fluid Mech 1970;42(3):471–89.
[72] Fornberg B. Steady viscous flow past a circular cylinder up to Reynolds number 600. J Comput Phys 1985;61:297–320.
[73] D'Alessio SJD, Dennis SCR. A vorticity model for viscous flow past a cylinder. Comput Fluids 1994;23(2):279–93.
[74] Yang HH, Seymour BR, Shizgal BD. A Chebyshev pseudospectral multi-domain method for steady flow past a cylinder, up to $Re = 150$. Comput Fluids 1994;23(6):829–51.
[75] Schlamp RJ, Pruppacher HR, Hamielec AE. A numerical investigation of the efficiency with which simple columnar ice crystals collide with supercooled water drops. J Atmosph Sciences 1975;32:2330–7.
[76] D'Alessio SJD, Dennis SCR. A method of domain decomposition for calculating the steady flow past a cylinder. J Eng Math 1994;28:227–40.
[77] Karniadakis GE, Triantafyllou GS. Frequency selection and asymptotic states in laminar wakes J Fluid Mech 1989;199:441–469.
[78] Schumm M, Berger E, Monkewitz PA. Self-excited oscillations in the wake of two-dimensional bluff bodies and their control. J Fluid Mech 1994;271:17–53.
[79] Peters U, Nischl H, Dwyer HA, Denk V. A numerical investigation of the Kármán vortex street in shear flow and comparison with experiments. In : Wagner S, Périaux J, Hirschel EH, editors. Proc 2nd European Comput Fluid Dyn Conf, Stuttgart. Chichester : Wiley, 1994. pp. 726–33.
[80] Nakai S, Okazaki T. Heat transfer from a horizontal circular wire at small Reynolds and Grashof numbers—I : pure convection. Int J Heat Mass Transfer 1975;18:387–96.
[81] Fand RM, Keswani KK. Recalculation of Hilpert's constants. J Heat Transfer, Trans ASME 1973;95:224–6.
[82] Eckert ERG, Soehngen E. Distribution of heat-transfer coefficients around circular cylinders in crossflow at Reynolds numbers from 20–500. Trans ASME 1952;74:343–7.
[83] Tsubouchi T, Masuda H. On the experimental formulae of heat transfer from single cylinders by forced convection. Rep Inst High Speed Mech, Tohoku Univ, Japan 1968;19:221–39.
[84] Gnielinski V. Berechnung mittlerer Wärme- und Stoffübergangskoeffizienten an laminar und turbulent überströmten Einzelkörpern mit Hilfe einer einheitlichen Gleichung. Forsch G Ing 1975;41(5):145–53.
[85] Fand RM, Keswani KK. A continuous correlation equation for heat transfer from cylinders to air in crossflow for Reynolds numbers from 10^{-2} to 2×10^5. J Heat Mass Transfer 1972;15:559–62.
[86] Schmidt E, Wenner K. Wärmeabgabe über den Umfang eines angeblasenen geheizten Zylinders. Forsch G Ing 1941;12(2):65–73.
[87] Douglas WJM, Churchill SW. Recalculation of data for convective heat transfer between gases and single cylinders with large temperature differences. Chem Eng Progress 1956;52(18):23–8.
[88] Gersten K, Herwig H. Impuls- und Wärmenübertragung bei variablen Stoffwertern für die laminare Plattenströmung. Wärme- Stoffübertragung 1984;18:25–35.
[89] Wehle F, Brandt F. Einfluss der Temperaturabhängigkeit der Stoffwerte auf den Wärmeübergang an der laminar überströmten ebenen Platte. Wärme- Stoffübertragung 1982;16:129–36.
[90] Herwig H, Wickern G. The effect of variable properties on laminar boundary layer flow. Wärme- Stoffübertragung 1986;20:47–57.
[91] Herwig H. Näherungsweise Berücksichtigung des Einflusses variabler Stoffwerte bei der Berechnung ebener laminarer Grenzschichtströmungen um zylindrische Körper. Forsch G Ing 1984;50:47–57.